Int. J. Electrochem. Sci., 15 **(2020)** 2648 – 2658, doi: 10.20964/2020.03.60

International Journal of ELECTROCHEMICAL SCIENCE
www.electrochemsci.org

Pulse jet electrodeposition of nanocrystalline copper and its application as an electrical discharge machining electrode

Hui Fan[1,], Yangpei Zhao[2], Jie Jiang[3], Shankui Wang[1], Wei Shan[1], Rulin Ma[1]*

[1] School of Mechanical and Electrical Engineering, Jiangsu Normal University, Xuzhou, 221116, China
[2] Jiang su Jiangzhu Institute, Xuzhou, 221116, China
[3] Jiangsu Key Laboratory of 3D Printing Equipment and Application Technology, Nantong Institute of Technology, Nantong, 226002, China
[*]E-mail: xzfanhui@163.com

Received: 25 November 2019 / *Accepted:* 7 January 2020 / *Published:* 10 February 2020

A nanocrystalline copper electrode material was fabricated using the pulse jet electrodeposition method on a stainless steel rod. The microstructure evolution and grain size were examined using scanning electron microscopy and X-ray diffraction. The nanocrystalline copper had a fine microstructure comprising nanosized grains with a size of 28 nm at a peak current density of 400 A/dm^2 and a pulse duty circle of 1:6. An electrode material mass loss experiment was conducted between the nanocrystalline copper electrode prepared by pulse jet electrodeposition and a conventional electroformed coarse copper electrode. The results show that the relative mass loss factor of the pulse jet electrodeposited copper electrode was obviously lower than that of electroformed coarse copper and reached a minimum value of 0.25% with an applied EDM peak current density of 3 A /dm^2.

Keywords: Electrode performance; pulse jet electrodeposition; nanocrystalline copper

1. INTRODUCTION

Electrical discharge machining (EDM) is a special machining technology that employs electrical corrosion to corrode conductive metals [1-6]. In the machining of the cavity of injection moulds or other moulds, the EDM technology is widely used because of its high machining precision and ability to process hard materials. The preparation of the electrode material is very important because during the corrosion of the work piece, the electrode can also be corroded, which easily influences the shape and dimensional accuracy of the target workpiece. Usually, to process a cavity in a mould, 3-4 electrodes are often needed [7-9]. The preparation of new electrodes is costly in terms of expense and time, thus affecting the processing efficiency. Therefore, reducing the electrode erosion loss during the EDM process is of great significance.

Common materials for electrodes include copper and its alloys, graphite, cast iron and steel. Electroformed copper is often used as an EDM electrode material because of its good conductivity and simplicity that enable the fabrication of precise and complex electrode shapes. However, due to a low melting point and low hardness, conventional electroformed copper cannot prevent electrode erosion loss during the procedure. As an effort to decrease the electrode mass loss and improve the electrode anti-electrical corrosion performance, researchers are focusing on creating new electrode material forming methods and changing the material composition. These efforts include powder metallurgy, high-temperature synthesis, and composite electrodeposition [1, 2]. In recent years, studies have mainly concentrated on a method of preparing copper composite materials to prepare EDM electrodes. Li prepared TiB_2 particle-reinforced copper matrix composites and researched the influence of the TiB_2 particle content on the electrode material microstructure and mechanical properties [7, 8]. Qiu employed a self-propagating high-temperature synthesis method to prepare Cu/TiB_2 as an electrode material, which had an erosion rate much lower than that of a common copper electrode [9].

Jet electrodeposition is a newly developed electrodeposition technology [1]. It has good localization and can generate a special nanocrystalline structure through the combination of a flow field and an electric field. According to the reported literature [10-20], copper parts with complex shapes and nanocrystalline microstructures can be prepared using jet electrodeposition. Based on the existing research [18-25], nanocrystalline materials have dense microstructures and good mechanical properties. The preparation of nanocrystalline electrode materials by jet electrodeposition is expected to improve the performance of electrodes and reduce the mass loss of electrodes during processing. However, to date, few works have been reported in this regard. Additionally, the mechanism for the effect of jet electrodeposition technical conditions on the electrode material performance is not yet clear.

In this paper, a nanocrystalline copper material was prepared by pulse jet electrodeposition, and the performance of the fabricated electrodes was compared with that of conventional electroformed copper. The electrode mass loss test was carried out on EDM tools.

2. MATERIALS AND METHODS

As shown in Fig. 1, an experimental jet electrodeposition system was employed to produce a nanocrystalline material, and the system included a computer-controlled worktable, jetting nozzle and pulse power source. The stainless steel was cut into substrates with dimensions of 80 mm×20 mm×1.5 mm. Electrodeposition was conducted using a pulsed current. The electrolyte composition and experimental conditions are listed in Table 1.

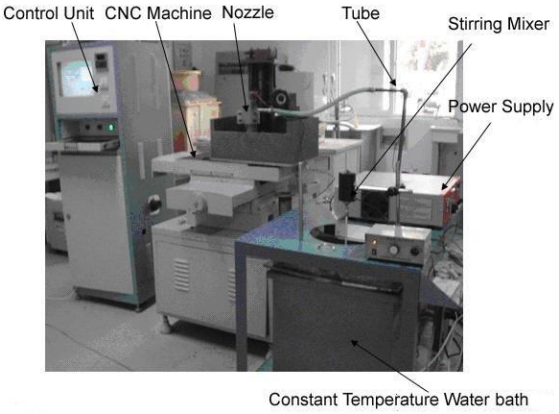

Figure 1. Experimental apparatus for jet electrodeposition process

The electrode mass loss experiment was carried out on a ROBOFORM35 CNC EDM precision machine tool using kerosene as the working medium. The electrode mass loss test conditions are provided in Table 2. Negative polarity machining was used, where the electrode for the nanocrystalline copper and the electroformed copper was connected to the positive pole of the power source, and the work piece was connected to the negative pole of the power source. The work piece was made of a stainless steel rod with a diameter of 4 mm.

The test electrodes and work pieces were cleaned with water and acetone before and after processing. After drying, the electrode and work piece mass variations were measured using an electronic balance (precision 0.1 mg). The relative loss was used to determine the galvanic corrosion resistance capacity of the electrode, as the relative quality loss factor is equal to mg / MG×100%, in which mg and MG represent the mass loss of the electrode and work piece, respectively.

Table 1. Electrolyte composition and experimental conditions

Electrodeposition bath and parameters	Composition and condition
$CuSO_4$•$5H_2O$	250 (g/L)
H_2SO_4	50 (g/L)
Temperature	50 ± 2 ℃
Nozzle size	Rectangular (20 mm×1 mm)
Jet gap	5 mm
Electrolyte jet velocity	10 m/s
Scanning rate	1000 mm/min
Duty circle	1:2-1:6
PC current density	200-500 A/dm^2
Pulse frequency	5000 Hz
Deposition time	30 min

Table 2. EDM electrode mass loss experimental conditions

Parameters	Condition
Peak current	1-3 A
Pulse width t_{on}	50-200 μs
Pulse width t_{off}	100 μs
Processing time	20 min

3. RESULTS AND DISCUSSION

3.1. Influence of the electrodeposition conditions on the nanocrystalline copper microstructure

Fig. 2 shows the influence of the peak current density on the evolution of the deposited coating microstructures. As the peak current density increases in the range from 200 A/dm^2 to 500 A/dm^2, the deposit coating microstructures gradually become dense and uniform. In contrast, the deposit material produced with 400 A/dm^2 shows a much denser microstructure with fewer pores than the materials deposited at lower current densities. As shown in the high-magnification SEM image in Fig. 2d, the microstructure is composed of nanocrystalline particles sized between 30 and 50 nm when a peak current density of 400 A/dm^2 is used.

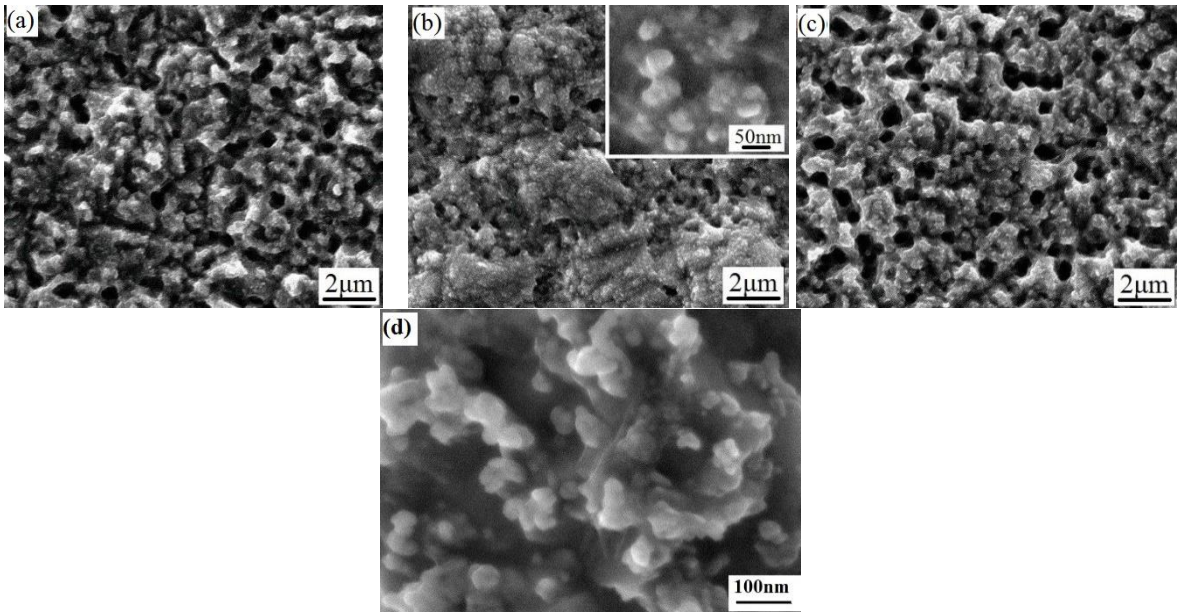

Figure 2. Microstructure variations with various peak current densities: (a) 300 A/dm^2, (b) 400 A/dm^2, and (c) 500 A/dm^2; (d) nanocrystalline grains at 400 A/dm^2

The grain size of the nanocrystalline coating was obtained with XRD analysis. From Fig. 3, as the peak current density rises from 200 A/dm^2 to 400 A/dm^2, the grain size decreases from 37 nm to 31 nm. With an increasing peak current density, the size decreases by 22% and attains the minimum grain

size. Then, as the peak current density continues to increase from 400 A/dm^2 to 600 A/dm^2, the size begins to increase and reaches a maximum of 71 nm when 600 A/dm^2 is applied. The change in the nanocrystalline grain size with increasing peak current density might be interpreted based on electrodeposition theory [10-13]. In general, the increase in current density can favourably promote the cathodic overpotential and the nucleation probability, hence favourably generating a strengthened microstructure and refined grains in the deposit.

However, once the current density exceeds 400 A/dm^2, the liquid mass transfer rate in the electrolyte cannot keep up with the metal ion consumption. The copper ions consumed by the reduction reaction at the cathode and solution interface cannot be supplemented in time, and the current density cannot be increased. Increasing the concentration polarization only results in an insufficient reduction of the metal ions. Therefore, the grain growth rate is faster than the nucleus formation rate, resulting in an increase in the grain size of the deposited layer with increasing current density. This relationship between the grain growth and nucleation can clearly explain the experimental phenomenon whereby the nanocrystalline grain size changes with increasing peak current density.

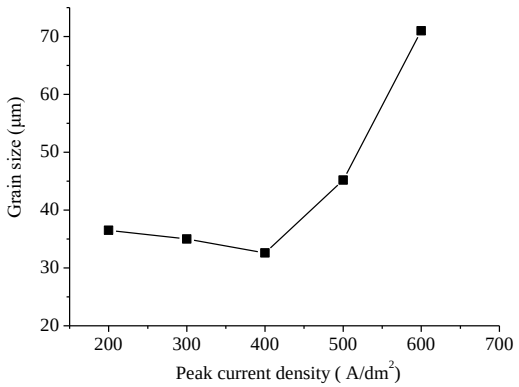

Figure 3. Effect of peak current density on the grain size of the deposited coating

Fig. 4 displays the microstructure of the deposited coating prepared for a range of duty cycles from 1:1 to 1:6 with a peak current density of 400 A/dm^2. As seen in the image, the coating contains a variety of structures, from a disordered and irregular distribution of large pores to a homogenous and fine microporous structure. With relatively large duty cycles of 1:2 or 1:3, the microstructure remains coarse, the formed pores are 3-4 μm long and have a worm-like shape and disordered distribution (Fig. 4 a, b), and there is a relatively low porosity of approximately 55%. As the duty cycle decreases to 1:6, additional pores appear, the shape of the pores becomes regular, and there is a relatively high porosity of approximately 71%. Moreover, the distribution of the porous structures are more homogeneous than that for the higher duty cycles. This improvement is related to the change in the pulsed duty cycle because if a lower duty cycle is applied, the pulse interval becomes longer, and additional metal ions are transported to the cathode to replace the consumed ions during the previous pulse [11]. This effect improves the restoration of the ion concentration and promotes the generation of seeds for the nucleation process. To further study the characteristics of the porous structure, a random region is selected in the

microstructure shown in Fig. 4d. It can be seen that a large number of extremely fine particles are arranged in a tight and orderly manner, forming a uniformly distributed microporous honeycomb structure. The micropore size is mostly below 100 nm, and the particle size is far less than 50 nm.

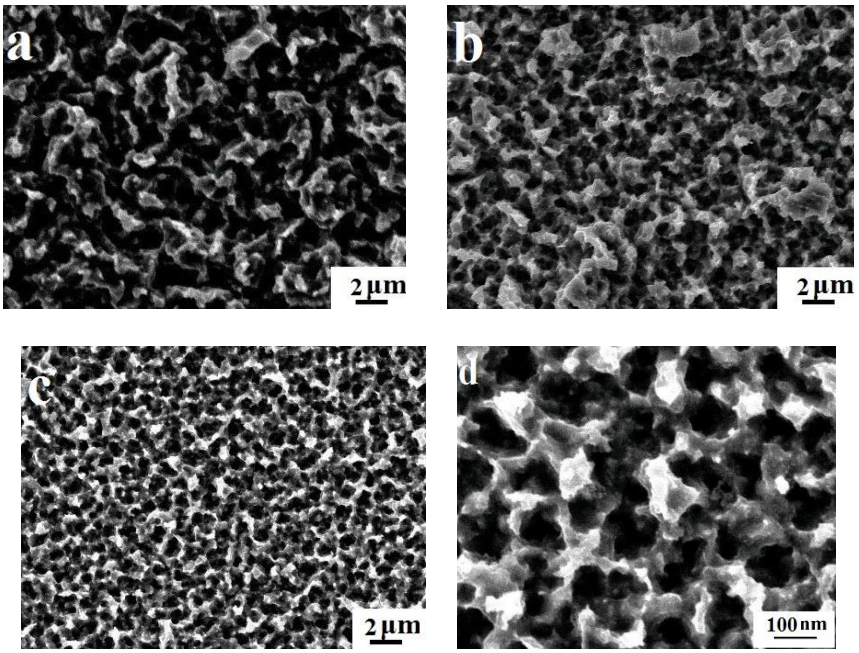

Figure 4. The cross-sectional morphologies of the coatings prepared with duty cycles of (a) 1:2, (b) 1:4, and (c) 1:6; (d) magnification of the image for a duty cycle of 1:6

Fig. 5 describes the effect of the pulse duty cycle on the grain size of the nanocrystalline coating. When the duty cycle is in the range of 1:2-1:7, the grain size decreases from 51 nm to 37 nm. As the duty cycle decreases, the grain size decreases by 27%, with the smallest grain size herein for a duty cycle 1:6. This variation trend also coincides with the observation of the cross-sectional morphologies of the coatings prepared using various duty cycles; with increasing duty cycle, the grain size of the nanocrystals gradually refine, and the structure gradually becomes compact. However, the duty cycle should not always be reduced because a duty cycle that is too small leads to a sharp reduction in the effective time of the current and restrains the efficiency of the coating deposition. In addition, a duty cycle that is too small, for example, 1:7, reaches its capacity and rarely improves the deposit quality. Therefore, the selection of an appropriate duty cycle should be considered based on its effect on the deposit quality and related deposition efficiency [11, 26-35].

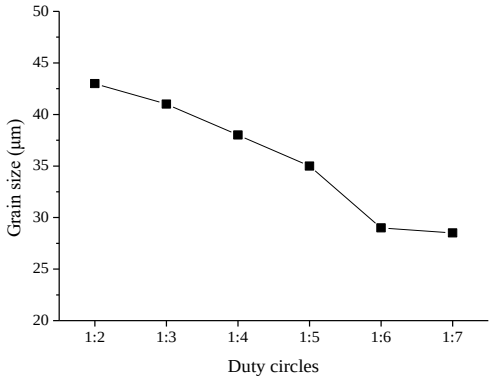

Figure 5. Effect of duty cycles on the grain size of the deposited coating

3.2. Electrode mass loss comparison analysis

Fig. 6 shows the relationship between the grain size and relative loss of the nanocrystalline copper. This shows that the nanocrystalline grain size has a significant effect on the electrode mass loss. The relative loss of the nanocrystalline copper increases with increasing grain size. When the grain size decreases from 78 to 28 nm, the mass loss of the copper electrode decreases from 10.3% to 7.8%, respectively.

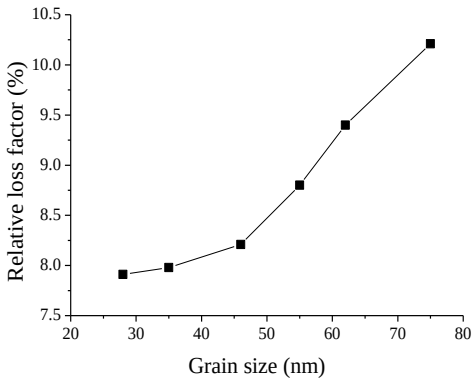

Figure 6. Effect of the grain size on the electrode mass loss

The effects of the peak current applied during the electrode mass loss test on the loss of the nanocrystalline jet electrodeposited copper electrodes and conventional coarse-grained electroformed copper were investigated, as shown in Fig. 7. It can be seen that the mass loss of the two kinds of copper electrodes have the same change trend with respect to the peak current density. This indicates that the mass loss of both electrodes decreases with increasing peak current, but apparently, the nanocrystalline copper electrodes have less corrosion loss than the coarse-grained electroformed copper electrodes. Additionally, when the peak current is in the range of 1-2 A, the peak current exerts little effect on the electrode mass loss. When the peak current increases from 2 A to 3 A, the electrode mass loss of the

nanocrystalline copper and coarse-grained copper varies greatly; the electrode mass loss of the nanocrystalline copper decreases from 9.43% to 0.43%, and the electrode mass loss of coarse-grained copper decreases from 10% to 1.56%. When the peak current increases from 3 A to 4 A, the mass loss decreases to 0.25% and 1.13%, respectively.

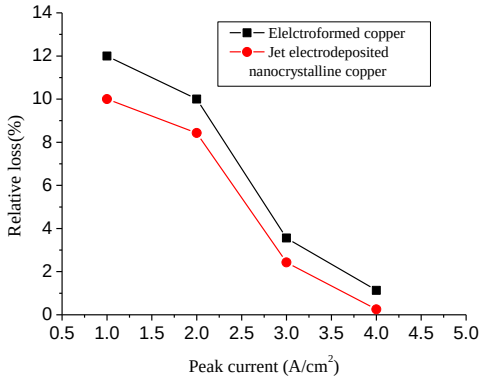

Figure 7. Effect of the peak current on the electrode mass loss

The effect of the pulse width applied during the electrode mass loss test on the loss of the nanocrystalline copper and conventional coarse-grained electroformed copper was investigated, as shown in Fig. 8. The mass loss of the nanocrystalline copper electrode decreases with increasing pulse width. When the pulse width increases from 50 μs to 200 μs, the electrode mass loss decreases from 0.95% to 0.25%, respectively. In fact, under a fixed current, upon increasing the pulse width, the number of pulse discharges per unit time would be decreased equivalently, thus reducing the influence of the discharge breakdown loss. When the peak current increases from 2 A to 3 A, the electrode mass loss of the nanocrystalline copper and coarse-grained copper varies greatly; the electrode mass loss of the nanocrystalline copper decreases from 9.43% to 0.43%, and the electrode mass loss of coarse-grained copper decreases from 10% to 1.56%. When the peak current increases from 3 A to 4 A, the mass loss decreases to 0.25% and 1.13%, respectively.

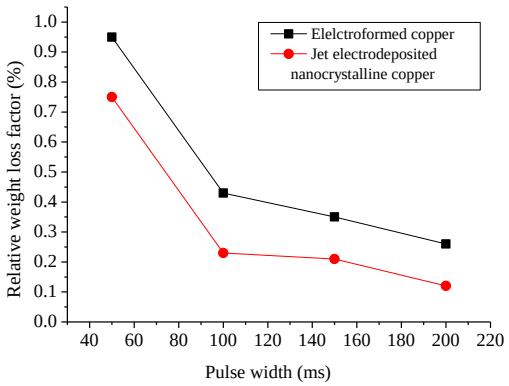

Figure 8. Effect of the pulse width on the electrode mass loss

At the same time, due to an increase in the pulse width, the electrode easily forms a covering by which the free carbon forms a carbon layer on the electrode surface and covers it. After the black carbon film is produced, the electrode surface is protected and the mass loss is reduced. As shown in Fig. 9, the surfaces of the nanocrystalline copper and electroformed copper electrodes are all covered with a dark layer. However, it seems there are different colour depths, as the nanocrystalline copper electrode seems dark. Additionally, the surface areas of the nanocrystalline copper and coarse-grained copper were analysed by energy dispersive spectrometry. From Table 3, it can be seen that the carbon content on the surface of the nanocrystalline copper electrode is obviously higher than that of electroformed coarse-grained copper, which coincides with the experimental observation from Fig. 9. The relative mass loss of the nanocrystalline copper electrodes is less than that of electroformed copper, which is due to the high content of C, Fe, Cr and Ni adsorbed on the surface of the nanocrystalline copper electrodes. These elements, especially C, cover the surface of the copper electrodes and correspondingly play an important role in protecting the copper electrodes, which has been verified by subsequent studies. [1, 36-38]

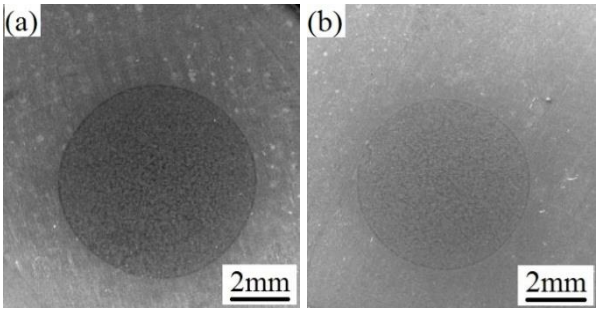

Figure 9. SEM Morphology of the copper electrode processing zone with (a) nanocrystalline copper and (b) conventional coarse-grained copper

Table 3. Chemical composition of the surface of the copper electrode (Wt %)

Element		C	Cu	Fe	Cr	Ni
Element Wt %	nanocrystalline copper	43.55	9.12	36.56	9.43	3.20
	Electroformed coarse copper	37.86	13.59	35.58	8.60	3.17

Fig. 10 shows the morphology of the electrical discharge machined area on the surface of the two electrodes. The two electrodes seem to have different surface colours. Energy spectrum analysis was conducted on the areas with carbon deposits for both the nanocrystalline copper and coarse-grained copper, and the results are displayed in Table 3. According to the statistics in Table 3, the surfaces of the copper electrodes are mainly composed of C, Fe, Cr and Ni. Among the elements, C is from the adsorption of the free carbon that separated from the kerosene working medium during the spark discharge process on the surface of the electrode; in contrast, the Fe, Cr and Ni are components of the workpiece, and their presence was caused by the sputtering of the workpiece onto the surface of the copper electrode after the melting and gasification that occur during the spark discharge process. According to Fig. 7 and Fig. 8, the relative mass loss of the nanocrystalline copper electrode is less than

that of the electroformed coarse grain copper. At same time, it can be seen that the carbon content on the surface of the nanocrystalline copper electrode is higher than that on the coarse-grained copper, and the copper content is lower than that on the coarse-grained copper. This may be due to the high content of C, Fe, Cr and Ni that is adsorbed on the surface of the nanocrystalline copper electrode. These elements, especially C, can cover the surface of copper electrodes and protect them [1, 2, 6]. The high content of C, Fe, Cr and Ni may provide improved protection.

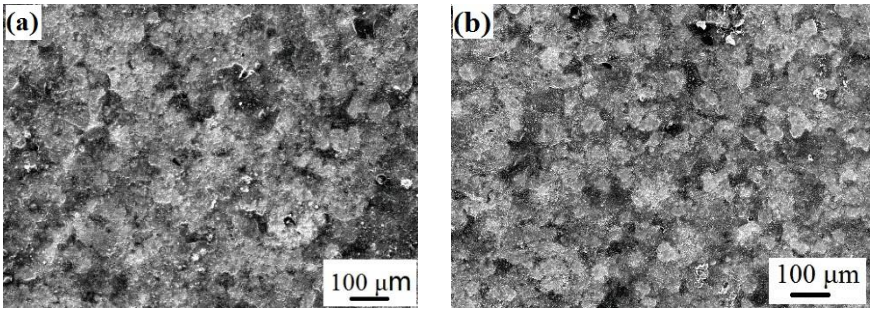

Figure 10. SEM Morphology of the copper electrode processing zone for the (a) nanocrystalline copper and (b) conventional coarse-grained copper

4. CONCLUSION

In this work, nanocrystalline copper was fabricated by using pulse jet electrodeposition. It was proven that the nanocrystalline coating using pulse current had an excellent deposition quality, including smooth surface morphology and consolidated microstructure. Nanocrystalline grains with a size of 28 nm were achieved with a peak current density of 400 A/dm^2 and a pulse duty circle of 1:6. In addition, the electrode mass loss of the nanocrystalline copper and electroformed coarse-grained copper was compared. The results show that the electrode mass losses of the nanocrystalline copper were less than those of the electroformed coarse-grained copper. The mass loss of the nanocrystalline copper reached a minimum value of 0.25% with an EDM peak current density of 3 A/dm^2, which is lower than that of the electroformed copper electrode.

ACKNOWLEDGEMENT
The National Natural Science Foundation of China (51305178), Jiang Su Natural Science Foundation (BK20181473), Xuzhou science and technology innovation project (KC19128), Top-notch Academic Programs Project of Jiangsu Higher Education Institutions (PPZY2015C251), the Priority Discipline Construction Program of Jiangsu Province (2016-9) supported this work.

References

1. H. M. Zaw, J. Y. H. Fuh, A. Y. C. Nee and L. Lu. *J. Mater. Process. Technol.*, 182 (1999) 89.
2. H. C. Tsai, B. H. Yan and F. Y. Huang. *Int. J. Mach. Tools Manuf.*, 245 (2003) 43.

3. O.Yilmaz and M.A. Okka. *Int. J. Adv. Manuf. Technol.*, 185 (2010) 51.
4. C. K. Yang , C. P. Cheng, C.C. Mai, A.C.Wang, J.C. Hung and B. H. Yan. *Int. J. Mach. Tools Manuf.*, 50 (2010) 1088.
5. M. Hamdi. *Int. J. Adv. Manuf. Technol.*, 76(2015) 329.
6. G. D'Urso, G. Maccarini and C. Ravasio . *Int. J. Adv. Manuf. Technol.,*72 (2014) 1287.
7. L. Li, X. T. Wei and G. M. Zheng. *Mater. Manuf. Process.*, 776 (2016) 31.
8. H. Fan, Y.P. Zhao, S.N. Cao, and Z.J. Li. *Mater. Trans.,* 60 (2019) 802.
9. N.S. Qu, K.C. Chan and D. Zhu. *Surf. Coat. Technol.*, 91 (1997) 220.
10. H. Fan, S.N. Cao, Y.P. Zhao and S.K.Wang. *Int. J. Electrochem. Sci.*, 14(2019) 8256.
11. H. Fan, Y.P. Zhao, S.N. Cao, and Z.J. Li. *Mater. Trans.,* 60 (2019) 802.
12. Y.W. Yao, S.W. Yao, L. Zhang and H.Wang. *Mater. Lett.*, 61 (2007) 67.
13. D.Q. Zhao, X. Jiang, Y.X. Wang, W. Duan and L. Wang. *Appl. Surf. Sci.*, 457 (2018) 914.
14. C.J. Xiao. *Surf. Eng.*, 34 (2018) 832.
15. M. Poorraeisi and A. Afshar. *Surf. Coat. Technol.*, 339 (2018) 199.
16. M.F. Morks, N.F. Fahim and A.A. Francis. *Surf. Coat. Technol.*, 201 (2006) 282.
17. H. Fan, Y.P. Zhao, S.K. Wang and R.L. Ma. *Mater. Res. Express,* 6(2019)1.
18. X.H. Zheng, J. Tan, Q. Zhang, M.Wang and L. Meng. *Surf. Coat. Technol.*, 311 (2017) 151.
19. D.R. Liu, Q. Zhang, Z.B. Qin, Q. Luo, Z. Wu and L. Liu. *Appl. Surf. Sci.*, 363 (2016) 161.
20. C.A. Huang, J.H. Chang , F.Y. Hsu and C.W. Chen. *Surf. Coat. Technol.*, 238 (2014) 87.
21. H. Yang and S.K. Wen. *Int. J. Mach. Tool. Manu.*, 40 (2000) 1065.
22. D. Zhu, W.N. Lei, N.S. Qu and H.Y. Xu. *CIRP. Ann. Manuf. Technol.*, 51 (2002) 173.
23. K.Y. Zhang, J.G. Liu and W. Xiao. *Mater. Lett.*, 193 (2017) 77.
24. S.K. Kumar and K. Biswas. *Surf Coat Technol.* 214 (2013) 8.
25. Y.H. Dong, K.J. Xu and S.G. Liu. *Chin. J. Nonferrous Met.*, 9 (1999) 370.
26. G.Y. Qiao, T.F. Jing and N. Wang. *Electrochim. Acta*, 51 (2005) 181.
27. H. Fan, Z.J. Li, Y.P. Zhao, S.K.Wang and S.N. Cao. *Int. J. Electrochem. Sci.*, 14(2019) 3326.
28. J. Tan, H. Song and X.H. Zheng. *Surf .Eng.*, 34 (2018) 861.
29. H. Kima, J.G. Kimb and J.W. Parkc. *Precis. Eng,* 51 (2018) 153.
30. F.F. Xia, W.C. Jia, C.Y. Ma, R. Yang, Y. Wang and M. Potts. *Appl. Surf. Sci.*, 434 (2018) 228.
31. M.S. Rajput, P.M. Pandey and S. Jha. *J. Manuf .Process*, 17 (2015) 98.
32. H. Fan, Y. Zhao, S. Wang and H. Guo. *Int. J. Adv. Manuf. Technol.*, 105 (2019) 4509.
33. Z.J. Tian, D.S. Wang, G. F. Wang, L. D. Shen, Z. D.Liu and Y. H Huang. *Trans. Nonferrous Met. Soc. China*, 20(2010) 1037.
34. Y. Wang, L. Shen, M. Qiu, Z. Tian, X. Liu and W. Zhuo. *J. Electrochem. Soc.*, 163(2016) 579.
35. M. Kunieda, R. Katoh, and Y. Mori. *CIRP. Annals*, 47(1998) 161.
36. W. Jiang, L.D. Shen and Q.X. Wang. *J. Alloys. Compd.*, 762 (2018) 115.
37. X. Liu, L.D. Shen and M.B. Qiu. *Surf. Coat. Technol.*, 305 (2016) 231.
38. J.F. Zhao, Y. Li, J. Zhang, C.Yu and Y. Zhang. *J. Mater. Process. Tech.*, 138 (2003) 475.